



# A higher-order mode coupler design for HEPS 166.6 MHz superconducting accelerating cavities

Xuerui Hao<sup>1,2</sup> · Zhongquan Li<sup>1</sup> · Fanbo Meng<sup>1</sup> · Pei Zhang<sup>1</sup>

Received: 6 September 2018 / Revised: 7 October 2018 / Accepted: 12 October 2018 / Published online: 1 November 2018

© Institute of High Energy Physics, Chinese Academy of Sciences; Nuclear Electronics and Nuclear Detection Society and Springer Nature Singapore Pte Ltd. 2018

## Abstract

**Purpose** The 166.6 MHz superconducting radio frequency cavities have been proposed for High Energy Photon Source (HEPS) storage ring. HEPS is a 6 GeV, 200 mA diffraction-limited synchrotron light source to be built in Beijing. Higher-order modes (HOMs) excited in 166.6 MHz SRF cavities have to be sufficiently damped in order to prevent coupled-bunch instabilities and to limit parasitic mode losses.

**Methods** A hybrid HOM damping scheme has been proposed. An enlarged beam pipe allows HOMs above beam pipe cutoff frequencies to propagate and subsequently be absorbed by dampers installed on the downstream beam pipe, while a petal-shaped coaxial structure extracts HOMs below beam pipe cutoff frequencies and subsequently damped by the specially designed coaxial filter.

**Results** HOM damping in cavities has been demonstrated by 3D simulations. The impedance of HOMs has been successfully reduced to be lower than the coupled-bunch instability threshold. In addition, no hard barrier multipaction has been observed and acceptable heat loss is obtained.

**Conclusions** In this paper, the hybrid HOM damping scheme has been demonstrated. Based on these studies, a prototype petal-loop structure and its associated filter are being fabricated.

**Keywords** Higher-order mode · Superconducting cavity · Impedance · Multipacting · Thermal analysis

## Introduction

Higher-order modes (HOMs) are components of the wake-field and can be excited by electron beam traversing an accelerating cavity. These modes may affect the beam stability as well as causing additional refrigeration load to the superconducting cavities if left unchecked. This is especially critical for high-current accelerators where impedance growth has to be well managed.

High Energy Photon Source (HEPS) is a 6 GeV diffraction-limited synchrotron light source with a beam current of 200 mA [1]. The fundamental RF frequency for the storage ring has been chosen to be 166.6 MHz in order

to accommodate novel injection schemes [2] as well as to compromise between the state-of-the-art kicker and RF technologies [3].

Due to the relatively low RF frequency, a quarter-wave shape has been adopted in order to keep the cavity in a manageable geometric size. During the R&D phase of HEPS, namely HEPS-TF, a 166.6 MHz superconducting radio frequency (SRF) proof-of-principle (PoP) cavity has been designed, fabricated and finally tested in IHEP with a success [4]. This was the first cavity to be built in order to maximize learning on cavity manufacturing techniques and surface treatment, regardless of HOM damping. While on the other hand, HOM suppression has been carefully studied and several HOM damping scheme are being investigated. This paper focuses on a hybrid damping scheme by using an enlarged beam tube to allow propagation of HOMs with above-cutoff frequencies and a specially designed petal-shaped coaxial structure to extract HOMs with below-cutoff frequencies. A specially designed HOM filter needs to be

✉ Xuerui Hao  
haoxr@ihep.ac.cn

<sup>1</sup> Institute of High Energy Physics, 19B Yuquan Road, Beijing 100049, People's Republic of China

<sup>2</sup> University of Chinese Academy of Sciences, Beijing 100049, People's Republic of China

added to the petal structure to facilitate fundamental mode suppression.

### HOM damping requirements

The enlarged beam pipe of the cavity can be treated as a circular waveguide. Generally, the TE and TM modes can be distinguished from the characterization of the electric and magnetic fields. The cutoff frequencies of the  $TM_{01}$  and  $TE_{11}$  modes for a circular waveguide are shown in Eqs. 1a and 1b: [5]

$$f_c(TM_{01}) = c \cdot \frac{2.405}{2\pi r} \tag{1a}$$

$$f_c(TE_{11}) = c \cdot \frac{1.841}{2\pi r} \tag{1b}$$

where  $c$  is the speed of the light and  $f_c$  is the cutoff frequency. As shown in Table 1, the first monopole HOM frequency is 464.875 MHz, and the first dipole HOM frequency is 431.266 MHz. As shown in Fig. 1, the radius of the tube needs to be 260 mm to extract all HOMs. 166.6 MHz cavity is using superconducting technology. If a large bundle tube structure with a radius of 260 mm is used, it will cause serious heat leakage problems, and the niobium is expensive and difficult to process, which causes serious economical expenses and mechanical performance problems. Therefore, we proposed a hybrid damping scheme where high-frequency modes will propagate through the beam pipe and low-frequency modes will be extracted by couplers. In this case, the beam pipe size dimension has been chosen to be 150 mm in radius. The bare cavity geometry is shown in Fig. 2.

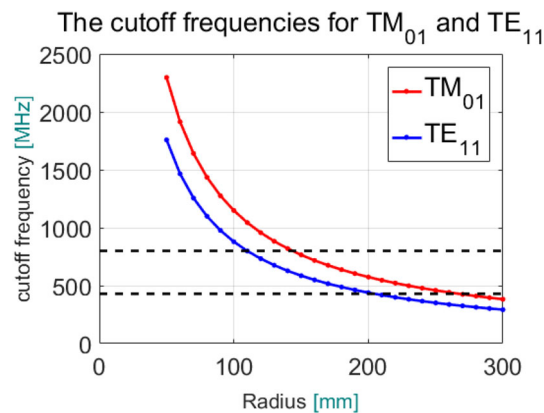


Fig. 1 Cutoff frequencies for  $TE_{11}$  and  $TM_{01}$  modes in a circular waveguide with various radii

HOMs of the enlarged tube cavity have been simulated by using CST MWS [6]. The results are listed in Table 1. Each mode has been converged to a determined frequency error value. The  $R/Q$  is calculated by using Eqs. 2a and 2b [7]:

$$\text{Monopole: } \frac{R}{Q} [\Omega] = \frac{|V|^2}{\omega \cdot U} \tag{2a}$$

$$\text{Dipole: } \frac{R}{Q} [\Omega/m] = \frac{1}{a^2} \cdot \frac{c}{\omega} \cdot \frac{|V|^2}{\omega \cdot U} \tag{2b}$$

where  $V$  is the cavity voltage,  $U$  is the stored energy in the cavity,  $a$  is the transverse beam offset,  $\omega/2\pi$  is the modal frequency and  $c$  is the speed of the light.

There are two impedance thresholds listed in the Table 1. The current RF system has five 166.6 MHz SRF systems as the fundamental. Firstly, considering each one of the five 166.6 MHz cavities have exactly same HOM frequencies, in

Table 1 RF result for the 166.6 MHz enlarged tube cavity

Mode	Freq. (MHz)	$R/Q$ ( $\Omega$ )	Equally distributed $Z^{th}$ ( $\Omega$ )	Total $Z^{th}$ ( $\Omega$ )
M2	464.875	67.3	8.6E+04	4.3E+05
M3	699.828	38.5	5.6E+04	2.8E+05
M4	923.110	3.9	4.2E+04	2.1E+05
M5	1198.746	9.1	3.2E+04	1.6E+05
Mode	Freq. (MHz)	$R/Q$ ( $\Omega/m$ )	$Z^{th}$ ( $\Omega/m$ )	$Z^{th}$ ( $\Omega/m$ )
D1.1	431.266	352	2.65E+06	5.3E+05
D1.2	432.308	387	2.65E+06	5.3E+05
D2.1	638.853	436	2.65E+06	5.3E+05
D2.2	640.534	448	2.65E+06	5.3E+05
D3.1	880.127	352	2.65E+06	5.3E+05
D3.2	880.513	363	2.65E+06	5.3E+05
D4.1	1026.389	327	2.65E+06	5.3E+05
D4.2	1026.738	327	2.65E+06	5.3E+05

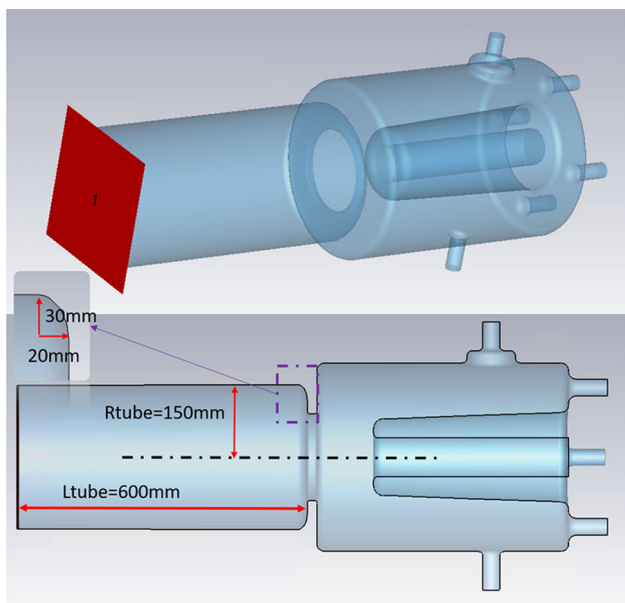


Fig. 2 The enlarged tube with cavity

other words, HOMs from all five cavities overlap with each other in the spectrum, thus share the total impedance budget. In this case, the impedance threshold per cavity is determined by [8] which is the most pessimistic situation thus giving the most strict damping requirements.

$$Z_{||,total}^{threshold} = \frac{1}{f_{||,HOM}} \cdot \frac{2 \cdot E_0 \cdot Q_s}{I_b \cdot \alpha \cdot \tau_z} \tag{3a}$$

$$Z_{x,y,total}^{threshold} = \frac{2 \cdot E_0}{f_{rev} \cdot \beta_{x,y} \cdot \tau_{x,y}} \tag{3b}$$

$$Z_{||}^{threshold} = \frac{Z_{||,total}^{threshold}}{N_c} \tag{3c}$$

$$Z_{x,y}^{threshold} = \frac{Z_{x,y,total}^{threshold}}{N_c} \tag{3d}$$

where  $Z_{||,total}^{threshold}$  and  $Z_{x,y,total}^{threshold}$  are total longitudinal and transverse impedance threshold,  $N_c$  is the number of cavities,  $f_{||,HOM}$  is the modal frequency,  $E_0$  and  $I_b$  are beam energy and beam current,  $Q_s$  is the synchrotron tune,  $\alpha$  is the momentum compaction factor,  $f_{rev}$  is the bunch revolution frequency,  $\beta_{x,y}$  is the  $\beta$  function,  $\tau_{x,y,z}$  are radiation damping time in three directions.

In either case, once the impedance threshold  $Z_{th}$  is calculated analytically, HOM damping requirement  $Q_{ext}^{th}$  can be obtained by Eq. 4a:

$$Q_{ext}^{th} = 2 \cdot \frac{Z_{th}}{R/Q} \tag{4a}$$

$$Z_{||,total}^{th} = \frac{1}{N_c} \cdot \frac{1}{f_{||,HOM}} \cdot \frac{2E_0 \cdot Q_s}{I_b \cdot \alpha_p \cdot \tau_z} \tag{4b}$$

$$Z_{x,y,total}^{th} = \frac{1}{N_c} \cdot \frac{1}{f_{rev}} \cdot \frac{2E_0}{I_b \cdot \beta_{x,y} \cdot \tau_{x,y}} \tag{4c}$$

$$Z_{||}^{th} = \frac{Z_{||,total}^{th}}{N_c} \tag{4d}$$

$$Z_{x,y}^{th} = \frac{Z_{x,y,total}^{th}}{N_c} \tag{4e}$$

where  $Z_{||,total}^{th}$  and  $Z_{x,y,total}^{th}$  are the total longitudinal and transverse impedance threshold;  $Z_{||}^{th}$  and  $Z_{x,y}^{th}$  are the longitudinal and transverse impedance threshold per cavity;  $E_0$  is the beam energy;  $Q_s$  is the Synchrotron tune;  $N_c$  is the number of cavity;  $I_b$  is the beam current;  $\alpha_p$  is the momentum compaction;  $\tau_{x,y,z}$  is the damping times;  $f_{rev}$  is the revolution frequency;  $\beta_{x,y}$  is the  $\beta$  function at linear section. This is the most pessimistic situation thus giving the most strict damping requirements, as denoted by ‘‘Equally distributed (E.Q.)’’ in the tables.

### The RF design

HOMs have been analyzed for the PoP cavity and reported in [9]. The goal of the petal-loop structure HOM coupler for 166.6 MHz SC cavity is to achieve HOMs extraction which below the enlarged beam tube cutoff frequency and suppression of the fundamental mode. In this section, the RF mode of the petal-loop structure and the double-notch filter are described.

### The petal structure

The petal-loop HOM coupler is mainly composed of the enlarged tube structure, a coaxial structure, a petal-loop structure and the double-notch filter, as shown in Fig. 3. An enlarged beam tube with a diameter of 300 mm was chosen, Under such conditions, the monopole cutoff frequency

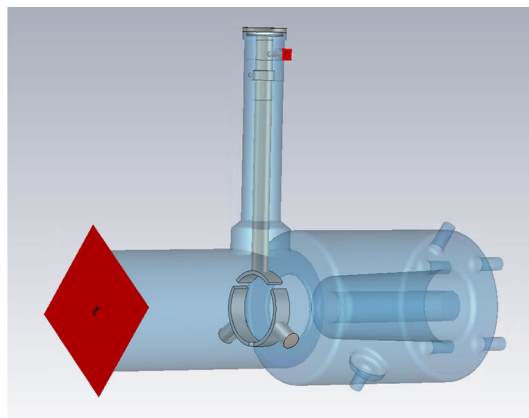


Fig. 3 The petal-loop structure of the HOM coupler

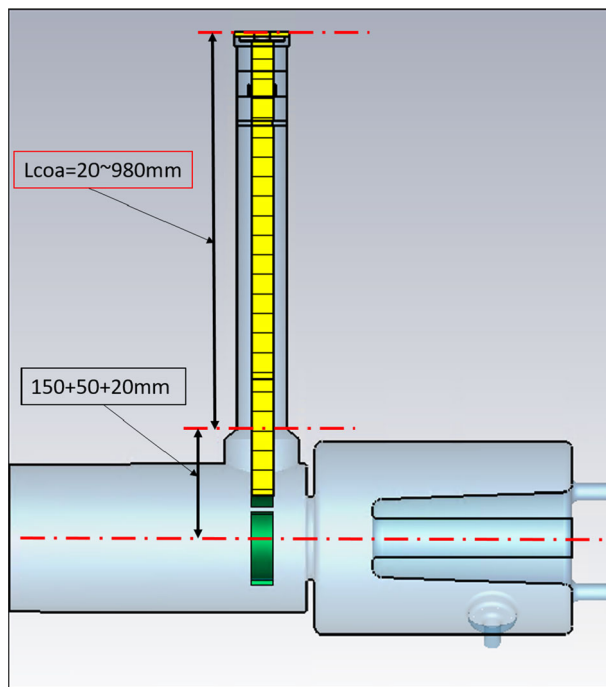


Fig. 4 The length of the waveguide

is 765 MHz and a dipole cutoff frequency is 586 MHz, which means that M2, M3 and D1 cannot be extracted from the enlarged tube. Thus these modes need to be extracted through the petal-loop structure, and their impedance thresholds are listed in Table 1.

The petal-loop structure is mainly composed of three parts: two petal structures connected to the inner face of the tube, a coaxial structure connected to one petal, and the double-notch filter structure. And the three petals form an annular structure. The advantage of the petal-loop is that the ring structure consisting of three petals has a high suppression of the fundamental model, but there is no inhibitory effect on the dipole mode. The notch filter is tuned to be at resonance with the fundamental mode of the cavity so as to suppress fundamental mode coupling to the HOM pickup probe.

The coaxial structure is the link between the petal-loop structure and the double-notch filter structure, and its length directly affects the structural performance. The length of the coaxial structure is mainly determined by three factors: the extraction based on the HOMs, the space occupied by the thermostat, and the surface power loss. This section is based on the extraction performance of higher-order modes to optimize the length of the coaxial structure, as shown in Fig. 4. However, the HOMs extraction capability is not synchronous, so it is necessary to make priority considerations for each HOM. The order of priority consideration is:  $M2 > D1 > M1 > M3, D2$ . And the length of the coaxial structure ranges from 20 to 980 mm. As shown in Fig. 5, the

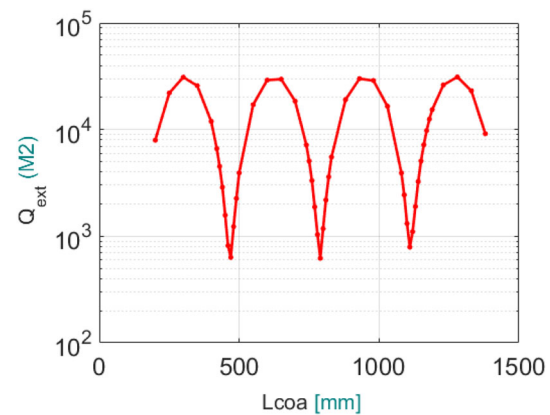


Fig. 5 The relationship between  $L_{coa}$  with  $Q_{e2}$  [M2]

extraction of the first higher-order mode, M2, varies periodically with the length of the coaxial line. Therefore, the length selection range of the coaxial structure is reduced to the vicinity of the minimum point of the  $Q_{ext}$  extraction value. This calculation is chosen at the first trough position.

## The impedance

Based on the introduction of a ring-shaped petal heterostructure in a large beam tube, it is possible to bring about abnormal changes in the wake field impedance. The impedance distribution has been calculated by using ABCI-MP [10]. ABCI is a 2D software that is specifically used to calculate the wake field and impedance problems. However, it can only calculate rotationally symmetric structural models. The petal-loop structure is an asymmetrical structure, but the main cause of the impedance change is the loop structure formed by the petal structure. Therefore, the petal-loop structure model can be simplified to a structure in which a ring is added to the enlarge tube, the structure is shown in Fig. 7. The impedance distribution of the enlarge beam tube structure and the enlarge beam tube with loop structure will be calculated by ABCI. By comparison, it can be known whether the ring structure will cause serious impedance problems. It is then verified whether the petal-loop structure causes severe impedance problems [11,12].

Figures 6 and 7 are accomplished through software ABCI. The petal structure could only be simplified by adding a ring structure to the enlarged tube.

Figure 8 shows the real part of longitudinal monopole impedance. The red line indicates the impedance distribution of the large beam tube structure, and the black line indicates the impedance distribution of the ring-shaped structure. Figure 9 shows the real part of the transverse dipole impedance. Figure 8 shows that, compared with the big tube structure, the impedance of the ring structure only has a large influence on M4. And from Fig. 9, we can find D2 has a large change.

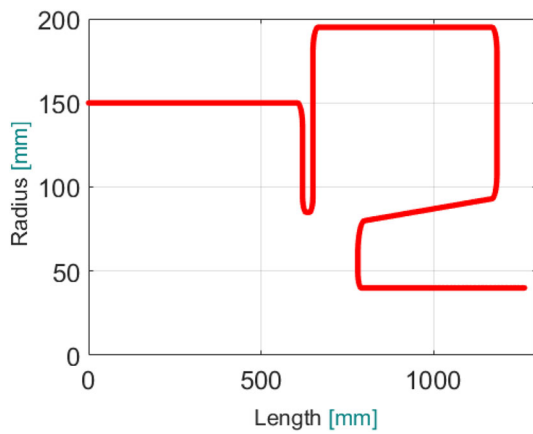


Fig. 6 The PoP structure by ABCI

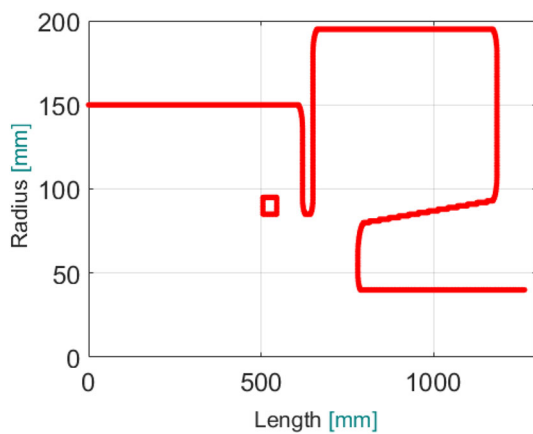


Fig. 7 The loop structure by ABCI

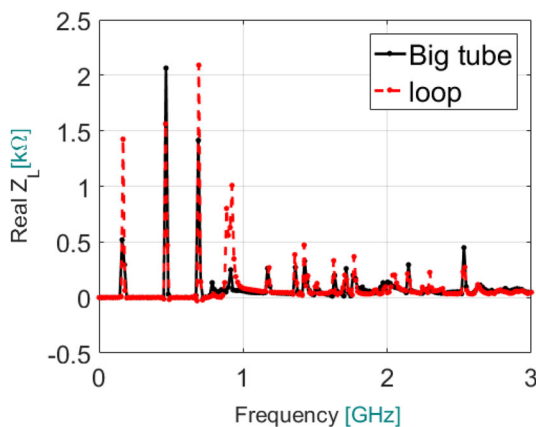


Fig. 8 Real part of longitudinal impedance-M(tube-hook)

Combined with the M4 and D2 conditions in Table 2, it can be seen that the changes brought by the two modes are all within the threshold.

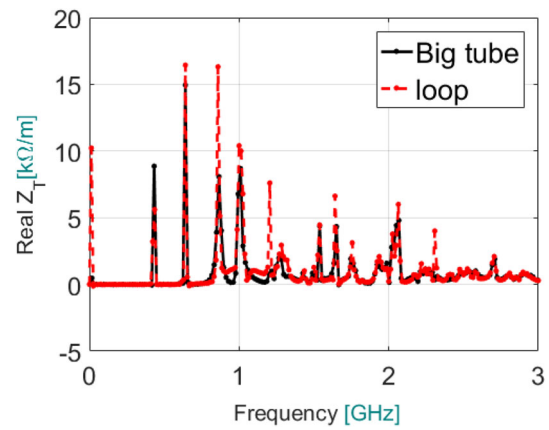


Fig. 9 Real part of transverse impedance-D(tube-hook)

Table 2 The RF result of SC cavity with HOM coupler

Mode	Freq. (MHz)	$R/Q$ ( $\Omega$ )	$Q_{ext}$	$Z$
M1	166.781	136	$1.1E+12$	
M2	465.187	84	738	$1.2E+05$
M3	698.756	34	1017	$6.8E+04$
M4	921.669	5	39	350

Mode	Freq. (MHz)	$R/Q$ ( $\Omega/m$ )	$Q_{ext}$	$Z$
D1-z	431.850	191	24510	$9.4E+06$
D1-y	432.881	452	29811	$2.7E+07$
D2-z	640.717	313	530	$3.3E+05$
D2-y	642.570	282	490	$2.8E+05$

### The damping results

The model structure has been selected and then the key parameters need to be optimized. In this process, the optimization software used is CST [6]. The results are shown in Table 2.

where the  $M$  stands for monopole and  $D$  in the name of dipole. Analyze the coupler extraction capability, the main reference parameter is  $Q_{ext}$ . In Table 2, it can be seen that the HOM coupler has reached the desired target for the high-order modes of the monopole, and there is room for upward adjustment, and the suppression of the fundamental mode also satisfies the requirements. For dipole's HOMs, where the effect of the first dipole mode extraction is considered by the length of the coaxial line and prioritized by the  $M2$  extraction, it can only meet the requirement of the growth time = 6 ms, while the other dipole modes, the extraction situation is satisfied.

### The MP for petal-loop structure

Multipacting (MP) is a phenomenon of resonant electron multiplication in which some specific inner surface areas of

a radio frequency (RF) device are repeatedly bombarded by electrons that gain energy from the RF field contained in the device [13]. And the multipactor (MP) in the HOM couplers of cavities is a known phenomenon that was studied already in a number of works [14]. Because of the energy deposition of MP electrons at bombardment sites, the cavity wall temperature may rise. This work is focused on multipacting in petal-loop structure; the main aim is to present the results of HOM coupler for 166.6 MHz SC cavity. The software used for MP simulations is CST Particle Studio which provides a particle tracking solver that uses the field from the eigenmode solver of Microwave Studio.

There are two ways to verify multipacting: the growth rate of secondary electrons and the secondary electron emission coefficient. The secondary electron growth rate can be calculated by Eq. 5, and the particle number changes with time in the calculation process through the particle studio; and the secondary electron emission coefficient can be obtained by Eq. 6, and can be known from Eq. 7. If  $SEY > 1$ , then the particle number is divergent, and accumulating over a period of time will cause electron avalanche to occur.

In the formula,  $N_0$  is the initial number of particles,  $\alpha$  is a growth factor and  $SEY$  is the secondary emission yield,  $n_{emission}$  is the secondary electron number, the  $n_{collision}$  is the primary electron number,  $I_{collision}$ ,  $I_{emission}$  are the primary incident current and the secondary outgoing current. When testing SEY, we cannot measure  $n_{emission}$ ,  $n_{collision}$  directly but get it by measuring  $I_{emission}$ ,  $I_{collision}$  [13].

$$\log N(t) = \log N_0 + \alpha t \tag{5}$$

$$\langle SEY \rangle = \frac{n_{emission}}{n_{collision}} = \frac{I_{emission}}{I_{collision}} \tag{6}$$

$$N_{e,m} = N_0 \langle SEY \rangle^m \tag{7}$$

Using secondary electrons as a function of time, one can quickly discover whether multipacting is occurring, but it is not possible to visually identify the cavity voltage and the degree of hazard during multipacting.

And we can use the SEY method to describe the multipacting problem. SEY's calculations need to consider the values of different materials under different accelerating cavity voltage, and analyze the possible multipacting situations. As shown in Fig. 11, the SEY has been calculation with different accelerating voltage in different treatment modes of Niobium.

In Fig. 10, the SEY characteristics of the two materials SEE Niobium 300 °C Bakeout and SEE Niobium Ar Discharge Cleaned are, respectively, introduced, and the dotted line portion is 0.9 for the line. SEY characterizes the ability of the surface of a material to be excited by electrons. SEY is different for different materials and different treatments for the same material surface.

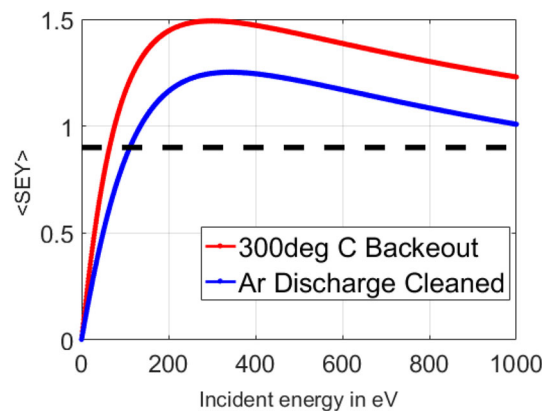


Fig. 10 SEY for Maerial: 300 °C bakeout versus Ar discharge cleaned

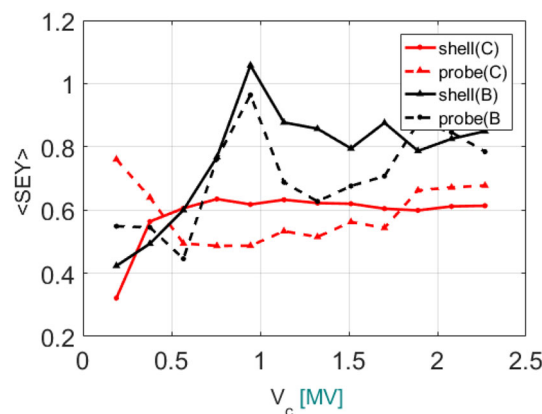


Fig. 11 The petal structure: 300 °C bakeout versus Ar discharge cleaned

In Fig. 11, the red line is made of SEE Niobium Ar Discharge Cleaned and the black line is made of SEE Niobium 300 °C Bakeout; the solid line indicates the coupler outer shell, and the broken line indicates the inner conductor and the petal structure. Focus only on the red line and find that  $SEY < 1$  at the accelerating voltage from 0 to 2.5 MV. It is consistent with the calculation results using the method of changing particles over time. Concerned about the black line portion, it was found that the dotted line portion has  $SEY > 1$  at accelerating voltage near 0.9 MV. It means that with SEE Niobium 300 °C Bakeout, multipacting occurs in the inner conductor portion at 0.9 MV cavity voltage. This part of the calculation is consistent with the particle number method, and finds the location where the multipacting occurs and the working voltage. Comparing the red and black lines, it can be known that the designed HOM coupler does not have a structural multipacting.

The 166.6 MHz superconducting cavity has a working accelerating voltage of 1.5 MV, and it is necessary to ensure the cleanliness of the materials in the later experiments.

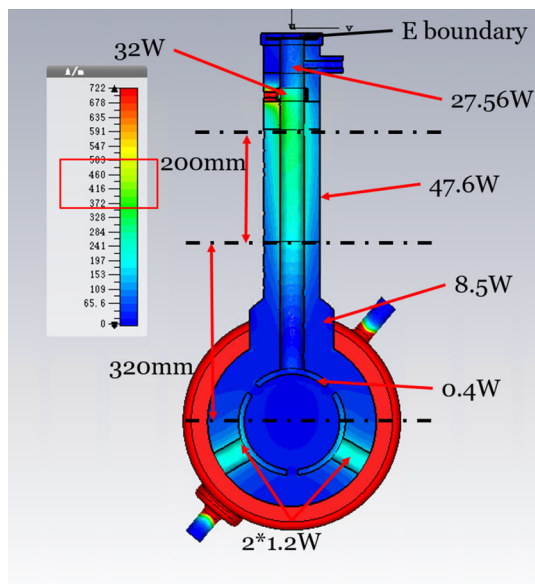


Fig. 12 Surface power loss distribution (LCoa = 480 mm)

### The thermal analysis

#### The thermal analysis for petal-loop structure

In the beam operating state, there may be a large surface power loss due to the location of the petal-loop structure. In severe cases, it may lead to an abnormal increase in local temperature, resulting in serious heat leakage and quenching of the superconducting cavity. Therefore, on the basis of the analysis of the static heat leakage and dynamic heat leakage of the comprehensive analysis structure, it is necessary to carefully design the selection of the structural materials and the position of the thermal anchor.

The length of the coaxial structure is mainly determined by the extraction capacity of the HOM, and the extraction performance of the HOM changes periodically, like Fig. 5. In order to determine its length, surface power loss also needs to be considered. Comparing the analysis of Figs. 12 and 13, it can be found that the magnetic field distribution has a large difference in the case where the HOMs extraction ability is the same. At LCoa = 480 mm, the magnetic field strength is at least three times that of LCoa = 810 mm. This leads to a sharp increase in surface power loss. Based on surface power loss considerations, we should choose LCoa = 810 mm.

The strength of the electromagnetic field distribution directly affects the surface power loss, and the choice of surface materials can also have a serious impact on the surface power loss. So the structural materials need to be selected: the resonant cavity, the large beam tube, and the two-part petal structure are made of niobium; the coaxial probe is made of copper; the coaxial structure is made of stainless steel or stainless steel copper plating material. The surface resistance and the skin depth are shown in Eqs. 8a and 8b:

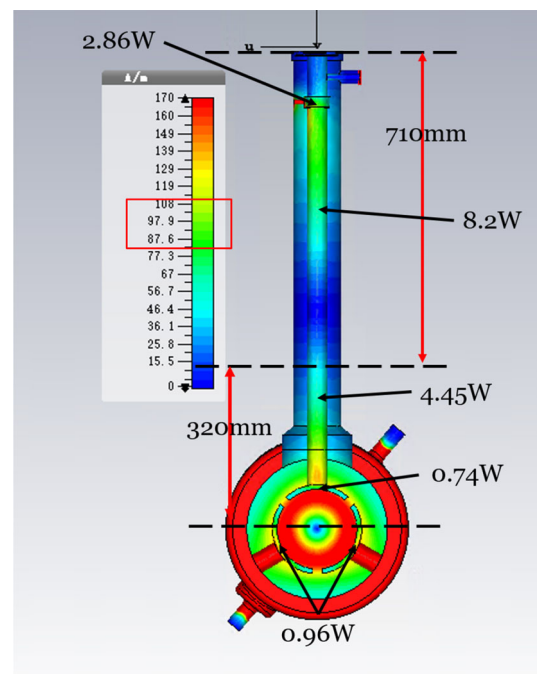


Fig. 13 Surface power loss distribution (LCoa = 810 mm)

$$R_s = \sqrt{\frac{\omega\mu_0}{2\sigma}} = \frac{1}{\sigma\delta} \tag{8a}$$

$$\delta = \sqrt{\frac{2}{\omega\mu_0\sigma}} \tag{8b}$$

$$q = -k\nabla T \tag{8c}$$

where  $R_s$  is the microwave surface resistance,  $\mu_0$  is the permeability of free-space, and  $\mu_0 = 4\pi \times 10^{-7}$  H/m.  $\sigma$  is the electric conductivity which related to the temperature;  $\delta$  is the skin depth;  $q$  is the heat flux,  $k$  is the thermal conductivity and the  $\nabla T$  is the temperature gradient.

First of all, we need to calculate the surface power loss of each part of the table under  $V_c = 1.5$  MV. In an environment with a temperature of 20 °C, the conductivity of the copper is  $5.9 \times 10^7$  S/m, the conductivity of stainless steel is  $7 \times 10^6$  S/m [15]; and the thermal conductivity of copper is 393.58 W/K/m, the thermal conductivity of stainless steel is 65.2 W/K/m.

From Eq. 8a, we could know, at the same temperature, the electrical conductivity of copper is an order of magnitude higher than that of stainless steel, so the surface loss will be much lower. However, copper has a better thermal conductivity than stainless steel which will cause more serious heat leakage. Therefore, on the outer conductor of the coaxial structure, stainless steel material or stainless steel copper plating material is used. Regarding the thickness  $d$  of the copper plating layer in stainless steel copper plating, it is necessary to satisfy  $d > 3\delta$  in practical applications. There-

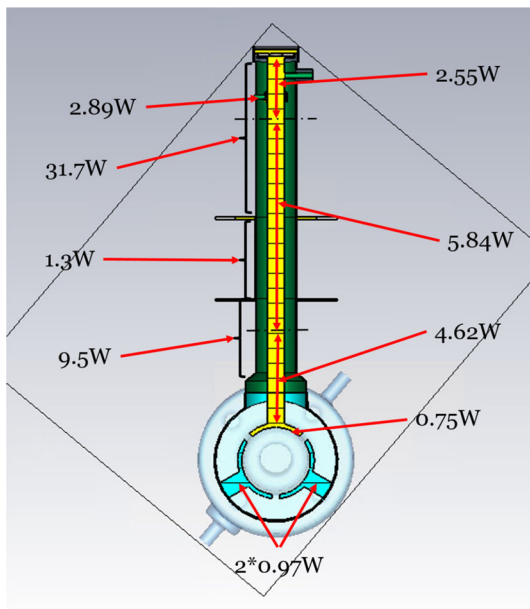


Fig. 14 Surface power loss distribution-steel ( $L_{coa} = 810$  mm)

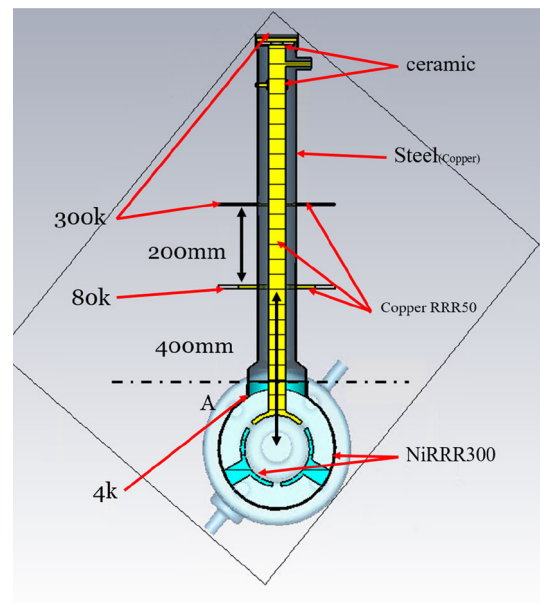


Fig. 16 Boundary conditions

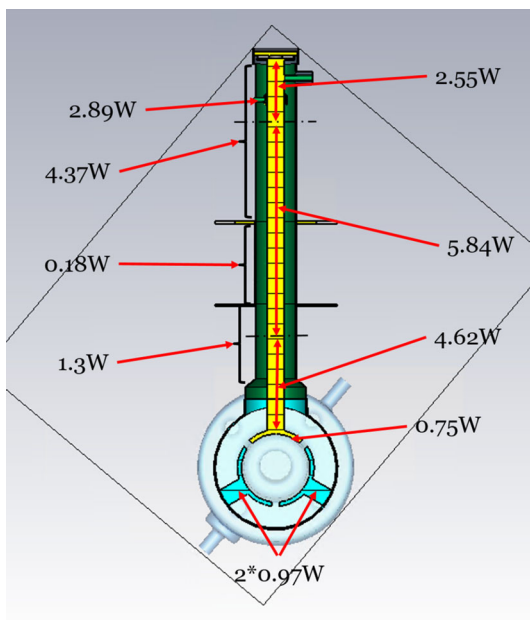


Fig. 15 Surface power loss distribution-cu ( $L_{coa} = 810$  mm)

fore, the thickness of the copper plating layer  $d$  is  $20 \mu\text{m}$  for the coaxial.

Coaxial structure using stainless steel, the result shown in Fig. 14. Using stainless steel copper plating, the results are detailed in Fig. 15. Comparing the two figures, it can be seen that the use of stainless steel copper plating material greatly reduces the surface loss. Therefore, the outer conductor of the structure is made of stainless steel copper plating material to reduce the heat load caused by the surface power loss.

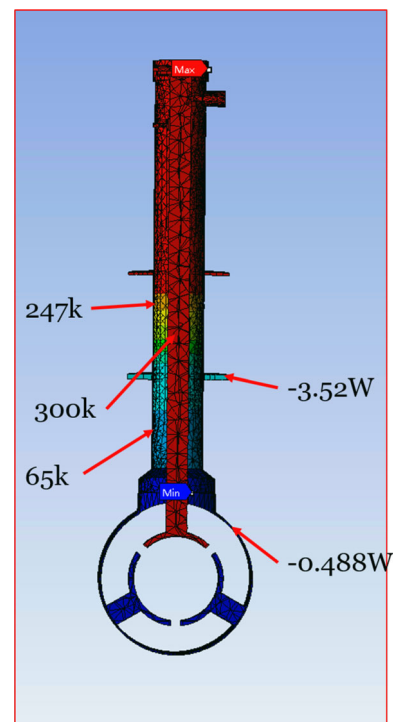
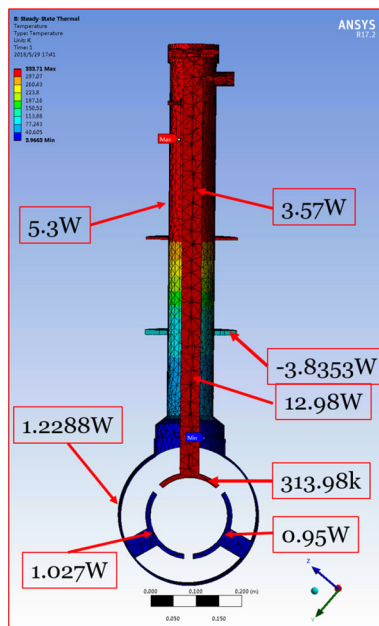


Fig. 17 Static heat leakage (Ansys)

The leakage heat calculation of the HOM coupler is calculated by the thermal analysis module in Ansys Workbench [16]. To calculate the heat leak problem, we need to define its boundary conditions. And according to the actual situation, set the initial temperature of each part of the structure and the position of the thermal anchor, as shown in Fig. 16.





**Fig. 18** Dynamic heat leakage (Ansys)

Calculate static heat loss under initial conditions and optimize thermal anchor position based on heat flow power, as shown in Fig. 17. In figure, the positive value of power indicates the release of heat, and the negative value of power indicates the absorption of heat. Based on this, it is possible to determine the initial temperature distribution and the heat flux absorbed by the cryogenic system and the thermal anchor. From the analysis in the figure, the 80 k thermal anchor absorbs 3.52 W of heat flow power under static leakage heat, while the large beam tube absorbs 0.48 W heat flow power.

Then, import the electromagnetic field and zoom in to  $V_c = 1.5$  MV to calculate the dynamic heat loss and the surface power loss due to beam current is 26.8 W. The result is shown in Fig. 18. The two-part petal structure produces 2 W power loss, the large beam tube produces 1.22 W power loss, and is absorbed by the 4 k cryogenic system; the power loss generated by the inner conductor is taken out of the low temperature system; and the temperature rise of the inner conductor structure is lower than 14 K.

## Summary

A hybrid higher-order mode (HOM) damping scheme has been proposed for HEPS 166.6 MHz superconducting cavities. HOMs with higher frequencies than the beam pipe cutoff are extracted from an enlarged beam pipe and sub-

sequently absorbed by the beamline HOM damper, while modes with lower frequencies are coupled through a specially designed petal-loop structure combined with a dedicated filter geometry to facilitate HOM propagation and accelerating mode suppression. The simulation demonstrated a satisfactory HOM damping if cavity frequencies are carefully tuned. In addition, no hard barrier multipaction has been observed from EM calculations and acceptable heat losses were indicated from thermal analysis. Based on these studies, a prototype petal structure and filter mockup are being fabricated.

**Acknowledgements** I would like to thank Dr. Zhang Xinying, Dr. Zheng Hongjuan from RF Group of Accelerator Division in IHEP for discussing design options. This work has been supported by the HEPS-TF project funding.

## References

1. G. Xu, X.H. Cui, Z. Duan et al., Progress of lattice design and physics studies on the high energy photon source, in *Proceedings of IPAC2018*, Vancouver, BC, Canada
2. G. Xu et al., On-axis beam accumulation enabled by phase adjustment of a double-frequency RF system for diffraction-limited storage rings, in *IPAC2016* (Busan, Korea) (2016). WEOAA02
3. P. Zhang et al., A 166.6 MHz superconducting RF system for the HEPS storage ring, in *Proceedings of IPAC2017*, MOPVA079, pp. 1049–1051
4. P. Zhang et al., The 166.6 MHz proof-of-principle SRF cavity for HEPS-TF, in *Proceedings of SRF2017*, TUPB034
5. D.M. Pozar, *Microwave Engineering*, 3rd edn. (Wiley, Hoboken, 2005)
6. CST Microwave, StudioÂ®. Ver. 2017, CST AG, Darmstadt, Germany (2017)
7. H. Padamsee, *RF Superconductivity for Accelerators*, ch. 9.3, 2nd edn. (Wiley, Hoboken, 2008), p. 174
8. F. Marhauser et al., HOM damped 500MHz cavity design for 3rd generation SR sources, in *Proceedings of PAC2001* (Chicago, USA, 2001), pp. 846–848
9. X. Hao et al., HOM damping with an enlarged beam tube for HEPS 166.6 MHz SC cavities, in *18th Int. Conf. on RF Superconductivity (SRF'17)*, Lanzhou, China, July 17–21, 2017, JACOW, Geneva, Switzerland (2018)
10. ABCI code. Ver. 12.5. <http://abci.kek.jp/abci.htm>. Accessed July 2017
11. G.V. Stupakov, Wake and impedance, in *AIP Conference Proceedings* (AIP, 2001)
12. L. Palumbo et al., Wake fields and impedance (2003). arXiv preprint [arXiv:physics/0309023](https://arxiv.org/abs/physics/0309023)
13. T. Khabiboulline et al., Multipacting in the ILC 1.3 GHz HOM Coupler (2015)
14. Y. Li, Comparative simulation studies of multipacting in higher-order-mode couplers of superconducting rf cavities. *Phys. Rev. Spec. Top. Accel. Beams* **17**(2), 022002 (2014)
15. M. Mario, Material properties for engineering analyses of SRF Cavities. Fermilab Specification
16. Ansys Workbench. <https://support.ansys.com/portal/site/AnsysCustomerPortal>. Accessed July 2017